Deterministically patterned biomimetic human iPSC-derived hepatic model via rapid 3D bioprinting

Xuanyi Ma[a,b], Xin Qu[b], Wei Zhu[b], Yi-Shuan Li[a], Suli Yuan[a], Hong Zhang[c], Justin Liu[d], Pengrui Wang[d], Cheuk Sun Edwin Lai[c], Fabian Zanella[e], Gen-Sheng Feng[f], Farah Sheikh[e], Shu Chien[a,1], and Shaochen Chen[a,b,1]

[a]Department of Bioengineering, University of California, San Diego, La Jolla, CA 92093; [b]Department of NanoEngineering, University of California, San Diego, La Jolla, CA 92093; [c]Chemical Engineering Program, University of California, San Diego, La Jolla, CA 92093; [d]Materials Science and Engineering Program, University of California, San Diego, La Jolla, CA 92093; [e]Department of Medicine, University of California, San Diego, La Jolla, CA 92093; and [f]Department of Pathology, University of California, San Diego, La Jolla, CA 92093

Contributed by Shu Chien, December 15, 2015 (sent for review November 9, 2015; reviewed by Gianfranco Alpini, Jordan Miller, and Wei Sun)

The functional maturation and preservation of hepatic cells derived from human induced pluripotent stem cells (hiPSCs) are essential to personalized in vitro drug screening and disease study. Major liver functions are tightly linked to the 3D assembly of hepatocytes, with the supporting cell types from both endodermal and mesodermal origins in a hexagonal lobule unit. Although there are many reports on functional 2D cell differentiation, few studies have demonstrated the in vitro maturation of hiPSC-derived hepatic progenitor cells (hiPSC-HPCs) in a 3D environment that depicts the physiologically relevant cell combination and microarchitecture. The application of rapid, digital 3D bioprinting to tissue engineering has allowed 3D patterning of multiple cell types in a predefined biomimetic manner. Here we present a 3D hydrogel-based triculture model that embeds hiPSC-HPCs with human umbilical vein endothelial cells and adipose-derived stem cells in a microscale hexagonal architecture. In comparison with 2D monolayer culture and a 3D HPC-only model, our 3D triculture model shows both phenotypic and functional enhancements in the hiPSC-HPCs over weeks of in vitro culture. Specifically, we find improved morphological organization, higher liver-specific gene expression levels, increased metabolic product secretion, and enhanced cytochrome P450 induction. The application of bioprinting technology in tissue engineering enables the development of a 3D biomimetic liver model that recapitulates the native liver module architecture and could be used for various applications such as early drug screening and disease modeling.

3D bioprinting | in vitro hepatic model | iPSC | tissue engineering | biomaterials

The liver plays a critical role in the synthesis of important proteins and the metabolism of xenobiotic; the failure of these functions is closely related to disease development and drug-induced toxicity (1). For these reasons, in vitro liver models have been extensively developed to serve as platforms for pathophysiological studies and as alternatives to animal models in drug screening and hepatotoxicity prediction (2–4). Human primary hepatocytes, considered one of the most mature liver cell sources, lose many liver-specific functions rapidly when cultured in vitro due to the great discrepancies between the native and culture environments (5, 6). In addition, the practical difficulties in obtaining liver biopsy samples from every patient further hinder their use in personalized liver models. Consequently, hepatocytes derived from human induced pluripotent stem cells (hiPSCs), with the potential to be patient specific and easily accessible, have been widely acknowledged as the most promising cell source for developing personalized human hepatic models (4, 7).

Many groups have reported monolayer differentiation of hiPSCs into hepatocyte-like cells (HLCs) and their ability to metabolize drugs (7–9). Nevertheless, hiPSC-derived HLCs are still considered immature in terms of many liver-specific gene expressions, functions, and cytochrome P450 (CYP) enzyme activities (7, 9). Major liver functions are tightly linked to the 3D assembly of hepatocytes with the supporting cell types from both endodermal and mesodermal origins in a hexagonal lobule unit. Current approaches to use HLCs for an in vitro liver model, however, are mostly limited to 2D culture or simple 3D spheroid cultures (3, 7, 10–14). The lack of a biomimetic microenvironment provided from the 3D interactions of parenchymal and non-parenchymal cell types along the hepatic differentiation stages may potentially be one of the limiting factors to functional maturation of the hepatic progenitor cells (HPCs), as well as the functional preservation of HLCs in vitro (15, 16).

Over the last decades, microtechnology tools have emerged to forge the advances in tissue engineering (3, 17–20). Although a majority of these microfabrication techniques are limited to the generation of simple 2D geometries with selected materials, digital light processing (DLP)-based 3D printing provides superior speed and scalability for the fabrication of complex 3D microstructure (21, 22). Moreover, this computer-aided, photopolymerization-based technique offers the flexibility to fabricate a great variety of 3D designs and incorporate a wide range of functional elements including live cells, biomolecules, and nanoparticles (23–25). Here we present the application of our customized DLP-based 3D bioprinting system to the development of a 3D hydrogel-based triculture model that possesses the physiologically relevant cell combination and microarchitecture. The DLP-based 3D bioprinting system allows us to embed hiPSC-HPCs and the supporting cells from both endothelial and mesenchymal origins in a 3D microscale hexagonal hydrogel construct, which progressively promotes cell

Significance

The great challenge to developing an in vitro liver model lies in the limitation of current approaches to recapitulate the sophisticated liver microenvironment contributed by the complex microarchitecture and diverse cell combination. We demonstrate an innovative advancement toward simulating natural complexity by integrating a rapid 3D bioprinting technology with tissue engineering to develop a microscale hepatic construct consisting of physiologically relevant hexagonal units of liver cells and supporting cells. The entire construct is fabricated within several seconds on minimal UV illumination. The model enables the structural and functional improvements of human induced pluripotent stem cell-derived hepatic progenitor cells and therefore can be used in early personalized drug screening and liver pathophysiology studies in vitro.

Author contributions: X.M., X.Q., W.Z., Y.-S.L., S.Y., S. Chien, and S. Chen designed research; X.M., X.Q., W.Z., Y.-S.L., S.Y., H.Z., and C.S.E.L. performed research; X.M., Y.-S.L., S.Y., C.S.E.L., and S. Chen analyzed data; X.M., X.Q., W.Z., Y.-S.L., J.L., P.W., F.Z., G.-S.F., F.S., S. Chien, and S. Chen wrote the paper; J.L. performed material synthesis; P.W. performed mechanical analysis of the materials; and F.Z. performed pluripotent stem cell generation and culture.

Reviewers: G.A., Central Texas Veterans Health Care System, Texas A&M University HSC College of Medicine, and Baylor Scott & White DDRC; J.M., Rice University; and W.S., Drexel University.

The authors declare no conflict of interest.

[1]To whom correspondence may be addressed. Email: shuchien@ucsd.edu or chen168@eng.ucsd.edu.

This article contains supporting information online at www.pnas.org/lookup/suppl/doi:10.1073/pnas.1524510113/-/DCSupplemental.

reorganization and realignment within the biomimetic architecture. Furthermore, we demonstrate the improvement of liver-specific gene expression, functions, and CYP induction in hiPSC-HPCs cultured in the 3D triculture model compared with those in conventional 2D monolayer culture and 3D HPC-only models.

To the best of our knowledge, this is the first report of an in vitro hepatic model that combinatorially mimic the several in vivo features of liver by providing a 3D culture environment for hiPSC-derived hepatic cells in triculture with supporting cells in a biomimetic liver lobule pattern. The application of DLP-based 3D bioprinting technology in tissue engineering enables the development of a 3D model for both the maturation and the subsequent maintenance of hiPSC-derived hepatic cells and hence can potentially be used for personalized medicine.

Results

A 3D Bioprinted Model That Patterns hiPSC-Derived Hepatic Cells and Supporting Cells in a Physiologically Relevant Design. To create a patient-specific hepatic model that mimics the native architecture and cell composition, we encapsulated hiPSC-derived hepatic cells and the endothelial- and mesenchymal-originated supporting cells in complementary patterns that mimic the hepatic lobule structure by photopolymerization of the hydrogel matrices (Fig. 1*A*). We first synthesized the biocompatible and photopolymerizable hydrogel solutions and examined the mechanical stiffness of these hydrogel matrices following light-induced polymerization (Fig. S1). Specifically, 5% (wt/vol) gelatin methacrylate (GelMA), with polymerized matrix stiffness similar to healthy liver tissues (26, 27), was chosen to support hiPSC-derived hepatic cells (Fig. S1). Glycidal methacrylate-hyaluronic acid (GMHA), which has been shown to promote endothelial cell proliferation and support vascularization (28), was mixed at 2% (wt/vol) with 5% (wt/vol) GelMA at a 1:1 ratio for encapsulating the supporting endothelial and mesenchymal cells.

Two patterns resembling the anatomical structures of hepatocytes and supporting cells were designed (Fig. 1*B*). The pattern dimensions were adjusted so that the bioprinted structures have lobule dimension approximated that of the human liver lobules in vivo. The patterns were transferred to both GelMA and GMHA hydrogels by DLP-based 3D bioprinting technology (Fig. S2), which used a digital micromirror device (DMD) chip to generate photomasks based on input digital patterns for photopolymerization of the hydrogel solutions as previously described (21, 23). To spatially pattern multiple types of cells and hydrogels, the digital masks were applied in a two-step sequential manner to create a first layer of hiPSC-derived hepatic cells supported by 5% (wt/vol) GelMA followed by a second complementary layer of supporting cells supported by 2.5% (wt/vol) GelMA and 1% GMHA (Fig. 1*A*).

By using this approach, we generated a 3D printed model of hiPSC-derived hepatic cells and the supporting cells representing the nonparenchymal cells from endothelial and mesenchymal origins in liver (Fig. 1*C*). The model measured 3 × 3 mm, with a thickness of ∼200 μm, and consisted of an array of liver lobule structure with the physiological dimensions (Fig. S3). Thus, this DLP-based two-step bioprinting approach provided an efficient and flexible way to create a 3D in vitro hepatic model that represents the in vivo hepatic structure.

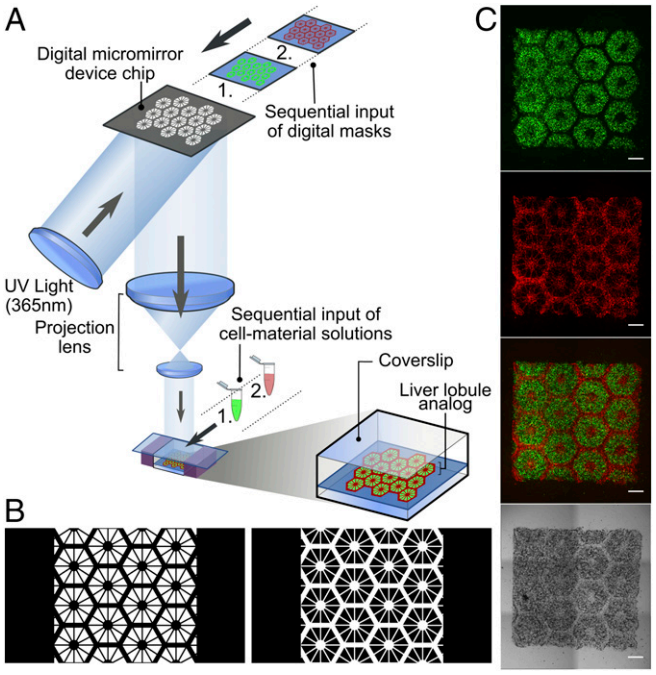

Fig. 1. 3D bioprinting of hydrogel based hepatic construct. (*A*) Schematic diagram of a two-step 3D bioprinting approach in which hiPSC-HPCs were patterned by the first digital mask followed by the patterning of supporting cells using a second digital mask. (*B*) Grayscale digital masks corresponding to polymerizing lobule structure (*Left*) and vascular structure (*Right*) designed for two-step bioprinting. The white patterns represent the light reflecting patterns for photo-polymerization. (*C*) Images (5×) taken under fluorescent and bright field channels showing patterns of fluorescently labeled hiPSC-HPCs (green) in 5% (wt/vol) GelMA and supporting cells (red) in 2.5% (wt/vol) GelMA with 1% GMHA on day 0. (Scale bars, 500 μm.)

3D Hydrogel Encapsulation at Hepatic Progenitor Stage Demonstrates a Sustained Higher Level of Albumin Production Compared with Encapsulation at Maturation Stage. hiPSCs generated from fibroblasts were induced to differentiate into hepatic lineage by a four-stage differentiation protocol modified from previous published methods (Fig. S4) (8). After differentiation initiation, cells at each of the four major stages, i.e., definitive endoderm, hepatic endoderm, hepatic progenitor, and further hepatic maturation, expressed stage-specific markers as confirmed by immunofluorescent staining (Fig. 2*A*). Hepatic specification was further confirmed by accessing the expressions of the four key liver-specific genes by quantitative PCR (qPCR) analysis (Fig. 2*B*). The expression levels of the hepatic lineage-specification gene hepatocyte nuclear factor 4α (HNF4a), fetal hepatic marker gene α-fetoprotein (AFP), and the more mature liver-specific genes transthyretin (TTR) and albumin (ALB) significantly increased as the differentiated cells matured over the various stages of hepatic differentiation (Fig. 2*B*). In particular, the expression levels of HNF4a, the fetal hepatic marker AFP, and TTR after 10 d of differentiation were much higher than those at endodermal stage, suggesting that differentiated cells after day 10 entered hepatic lineages (Fig. 2*B*) (13, 29, 30). Following hepatic lineage specification, cells entered hepatic progenitor stage, i.e., became HPCs after 12–14 d of differentiation, which further matured into HLCs after 17–19 d of differentiation (8, 30).

Cells at both hepatic progenitor and maturation stages, i.e., HPCs and HLCs, respectively, have demonstrated their potentials in organizing into vascularized liver buds (11, 13) and in the construction of in vitro models with simple geometry (10, 12, 14). To determine the stage of cells along the differentiation pathway that is more suitable for hydrogel encapsulation, HPCs and the relatively more mature HLCs were compared in terms of their albumin secretion time course following encapsulation in GelMA (Fig. 2*C*). Although neither cell type in 3D hydrogel culture was able to maintain the peak albumin secretion level, the encapsulated HPCs showed a more sustained secretion with a higher quantity (Fig. 2*C*). These findings suggest that HPCs may serve as a better candidate for in vitro liver model after several days of in vitro maturation.

Further characterization of hepatic progenitor cells immediately before encapsulation with flow cytometry showed that an average of 91% of cells were positive for both HNF4a and FoxA2, the hepatic specification markers (30), confirming their hepatic progenitor nature and purity (Fig. S5). Human umbilical vein endothelial cells (HUVECs) and the adipose-derived stem cells (ADSCs) were chosen as the supporting cells representing the endothelial and mesenchymal lineages for their primitive nature and their

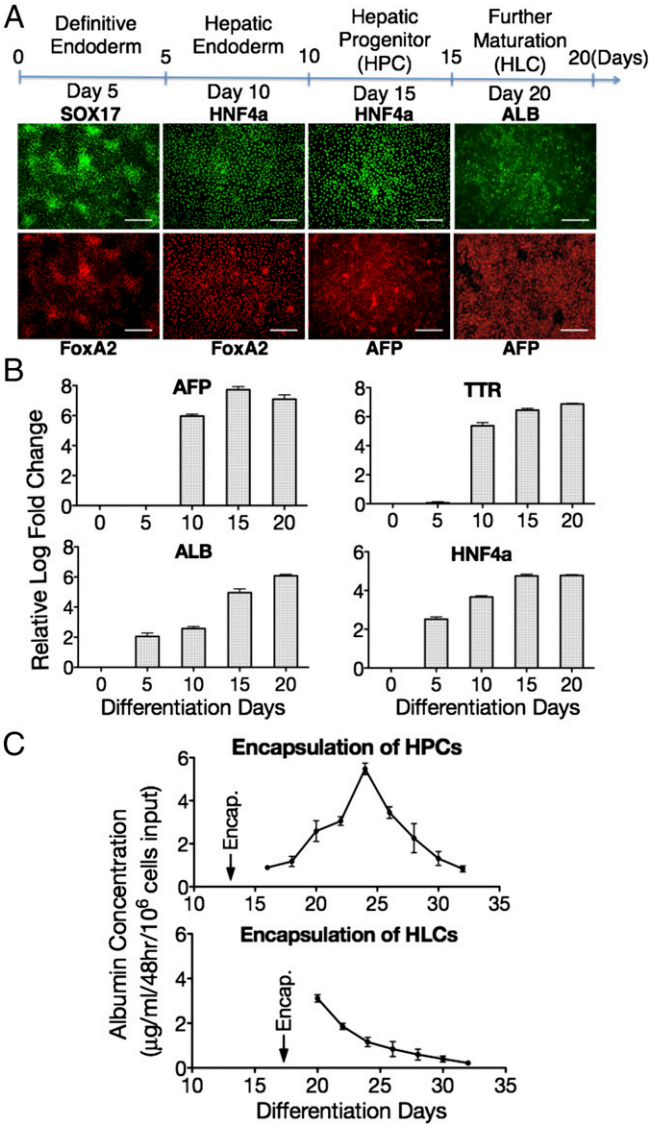

Fig. 2. hiPSC-derived hepatic cell preparation and comparison. (*A*) Four major hiPSC hepatic differentiation stages and the corresponding immunofluorescence images showing staining of the respective stage-specific markers. (Scale bars, 500 μm.) (*B*) Gene expression profiles by qPCR showing the expressions of ALB, HNF4a, TTR, and AFP of samples at hiPSC hepatic differentiation day (DD) 0, 5, 11, 16, and 20. All fold changes are relative to the expression level of hiPSCs. (*C*) Albumin secretion levels of HPCs (encapsulated on DD 13) and HLCs (encapsulated on DD 17) over time following their encapsulation by bioprinting. Albumin measurements were carried out beginning day 3 of encapsulation. Error bars represent SEM, and $n = 3$ for all data points.

potentials in forming functional vasculatures as shown and discussed in previous studies (11, 13, 31). Specifically, HUVECs were used over other endothelial cell types such as liver sinusoidal endothelial cells (LSECs) in consideration of the potential interaction between umbilical vein and fetal liver (29). ADSCs were used over other sources of mesenchymal stem cells for their easy availability from individuals and promising clinical applications (32). HUVECs and ADSCs were maintained in their respective culture media before encapsulation (Fig. S4).

In Vitro Structural Characterization of 3D Hepatic Triculture Model Showed Cell Reorganization and Realignment with Intrinsic Pattern Maintenance. To better understand the activities of cells after bioprinting, cell viability, cell migration, and intercellular interactions were characterized. The combinational effect of the entire bioprinting process, i.e., from cell suspension preparation to light-induced photopolymerization of cell suspension and material mixture, on cell viability was evaluated by viability assay on samples from day 0 to 7. Live and dead cells as characterized by calcein and ethidium homodimer-1, respectively, were quantified (Fig. S6). There were on average 76% viable cells when measured within 2 h following bioprinting (Fig. S6). No significant change was observed within the first 3 d, whereas after around a week, live cells accounted for 65% of the total population, suggesting that the majority of cells were still viable (Fig. S6).

We next observed the pattern maintenance and potential cell migrations within their patterns using fluorescently labeled hiPSC-HPCs (green) and supporting cells (red). Within the first day after bioprinting, cells appeared as individual spheroids patterned in their respective structures from the optical mask (Fig. 3 *A*, *B*, and *C, ii*). In about 3–7 d, the red fluorescently labeled HUVECs and ADSCs aligned along the hydrogel pattern of the matrix, demonstrating the sinusoid-like structures within liver lobule (Fig. 3 *A* and *B*, Fig. S7, and Movie S1). When observed under bright field, the patterns gradually became blurred over time, but were well distinguishable when observed under fluorescent channels, suggesting that the whole structure became an integrated construct without losing the intrinsic patterns designed for different cell types (Fig. 3*A*). Both hiPSC-HPCs and supporting cells were able to stay in their designated patterns for at least 10 d (Fig. 3*A*).

Over the course of 1 wk, hiPSC-HPCs formed aggregates with each other (Fig. 3*C*). Hepatocytes in aggregate or spheroid culture have been shown to be able to maintain viability and metabolic functions for a longer period than those in monolayer cultures, possibly due to the better retainment of in vivo hepatic morphological characteristics (33–36). To further study the hiPSC-HPC aggregates, immunofluorescent stainings were performed on E-cadherin, an epithelial marker that had been shown to protect primary hepatocyte from apoptosis (37), and intracellular albumin, a functional hepatic marker. Aggregates after 7 d of culture were stained positively for both E-cadherin and albumin, demonstrating functional spheroid formation (Fig. 3 *C, i* and *ii*). In addition, the average aggregate sizes of hiPSC-HPCs in 3D triculture model and hiPSC-HPC–only model were characterized and compared (Fig. 3*D*). The 3D triculture condition showed greater spheroid formation than the hiPSC-HPC–only condition by an average of around 10%. The larger spheroid size suggests a greater extent of cell junctions and potentially better hepatic functional performance (Fig. 3*D*) (34). Together, these results suggest that both hiPSC-HPCs and the supporting cells were able to reorganize in their designated pattern of the 3D triculture model over time and that the extent of cell–cell interactions of hiPSC-HPCs in 3D triculture model, as characterized by average spheroid size, was more than that in 3D HPC-only model.

The Enhancement of Liver-Specific Gene Expression and Functions of hiPSC-HPCs in the 3D Triculture Model. Although the greater extent of cell reorganization found in the 3D triculture model was encouraging, it was also important to explore the maturation level based on liver-specific gene expression and functions. To address this question, we first compared the relative expression levels of the hepatic marker genes in hiPSC-HPCs from 3D triculture model, hiPSC-HPC–only model, and the conventional 2D monolayer culture. The expression levels of the hepatic markers that are highly expressed in mature hepatocytes, i.e., HNF4a, TTR, and ALB, were higher in triculture condition compared with the other two. The expression levels of fetal hepatic marker AFP were not significantly different among the three conditions, but a trend of reduced expression level was observed in both the 3D HPC-only and 3D triculture model (Fig. 4*A*). Together, these findings showed a relatively more mature gene expression profile of hiPSC-HPCs in the 3D triculture model.

Next, we compared the anabolic and catabolic functional aspects of the hiPSC-HPCs in different models. The levels of albumin secretion by hiPSC-HPCs in different models over the period of

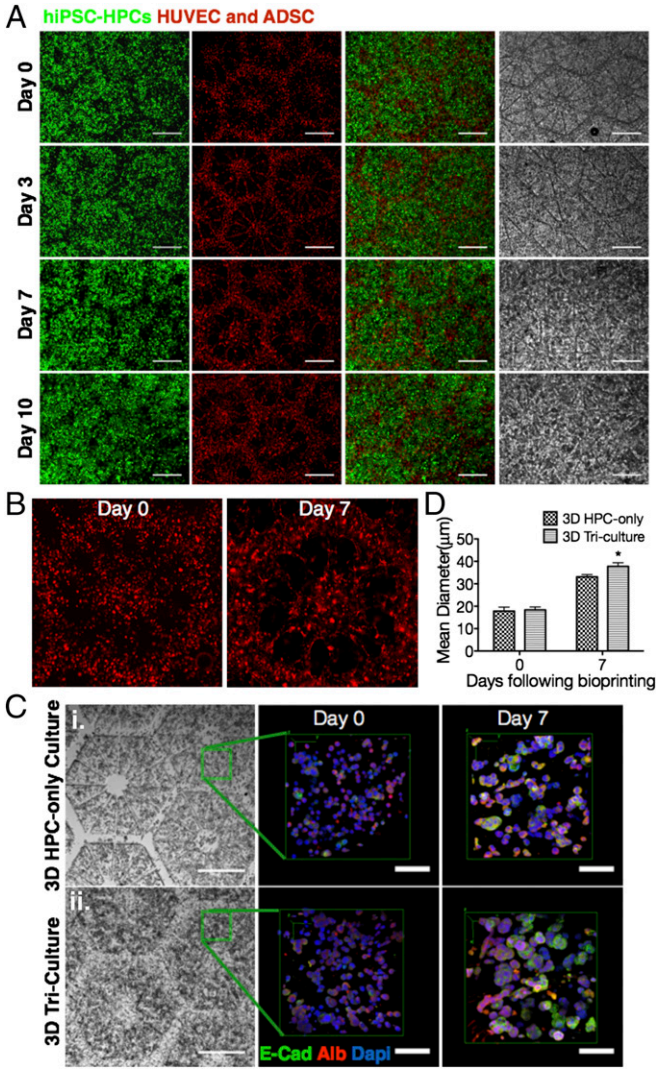

Fig. 3. Structural characterization of the hepatic model. (*A*) Fluorescent images (5×) of bioprinted construct consisting of tracked cells on day 0, day 3, day 7, and day 10. (Scale bars, 500 μm.) (*B*) Fluorescent images (enlarged) showing supporting cells arrangement on both day 0 and 7 following bioprinting. (*C*) Grayscale images (5×) and confocal immunofluorescence images (40×) showing albumin (Alb), E-cadherin (E-Cad), and nucleus (Dapi) staining of hiPSC-HPCs in (*i*) 3D HPC-only (with no supporting cells) constructs and (*ii*) in 3D triculture constructs. (Scale bars, 500 μm in bright field and 100 μm in fluorescent images.) (*D*) Bar graph showing mean diameters of spheroids within both HPC-only constructs and triculture constructs on day 0 and 7. Error bars represent SEM, and $n = 3$ for all data points.

19 d were compared (Fig. 4*B*). Albumin secretion declined in all three models following their respective peak, but hiPSC-HPCs in triculture model were able to maintain the highest level of secretion among the three conditions 5 d after bioprinting (Fig. 4*B*). Similarly, urea production levels from breaking down of amino acids were compared over time (Fig. 4*C*). The hiPSC-HPCs in triculture condition were shown to maintain the urea production level to a greater extent than the other two conditions (Fig. 4*C*).

Encouraged by the observed functional enhancement, we proceeded to investigate the expression levels of key enzymes in liver drug metabolism, i.e., CYPs in hiPSC-HPCs from the three experimental conditions. Specifically, we evaluated quantitatively the expression of the five key CYPs, CYP1A2, CYP2B6, CYP2C9, CYP2C19, and CYP3A4, which account for 60% of human drug oxidation (38). Among the five CYPs, the hiPSC-HPCs in 3D triculture model showed a significantly higher expression of CYP3A4, which is the most common CYP enzyme and estimated to be involved in the metabolism of approximately half the currently used drugs (Fig. 4 *D, i*) (39). Although not significant, hiPSC-HPCs in 3D triculture model demonstrated the highest average expression levels of CYP1A2, CYP2B6, CYP2C9, and CYP2C19 (Fig. 4 *D, ii–v*).

In addition to the evaluation on the baseline CYP expression levels without any drug treatment, the inductions of mRNA transcripts of the five CYPs in hiPSC-HPCs were further evaluated by treating samples with an inducer, rifampicin, which is a bactericidal antibiotic drug with potential risk of hepatotoxicity. The induction by rifampicin led to significant increases in CYP3A4, CYP2C9, and CYP2C19 expression levels in hiPSC-HPCs from the 3D triculture model culture compared with untreated controls (Fig. 4 *D, i–iii*). Such significantly increased CYP expressions from rifampicin treatment were not observed in hiPSC-HPCs from either 2D monolayer culture or the 3D-HPC–only model, although a trend of improved expression was also observed. The rifampicin treatment did not cause significant changes in CYP1A2 expression level of hiPSC-HPCs from any of the conditions (Fig. 4 *D, v*). This observation was expected as rifampicin was less likely to induce CYP1A2 as reported (40). However, rifampicin incubation also did

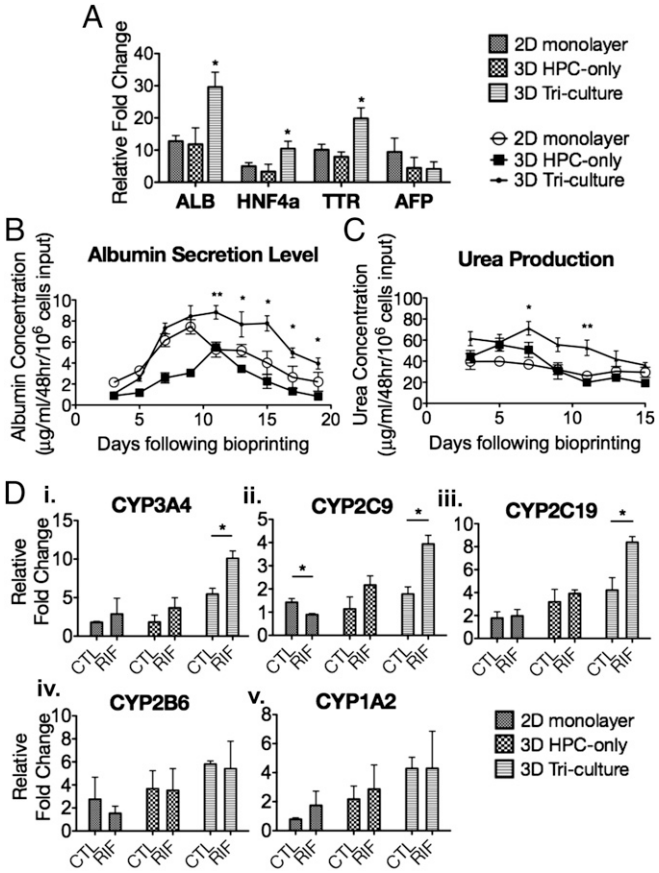

Fig. 4. Gene expression and functional characterization of the hepatic model. (*A*) Gene expression profiles comparing the ALB, HNF4a, TTR, and AFP expression levels of HPCs in 2D monolayer culture, 3D HPC-only culture model, and 3D triculture model on day 7 following bioprinting. (*B*) Albumin secretion levels of HPCs in three different conditions over time. (*C*) Urea secretion levels of HPCs in three different conditions over time. (*D*) Gene expression profiles showing expression levels of (*i*) CYP3A4, (*ii*) CYP2C9, (*iii*) CYP2C19, (*iv*) CYP2B6, and (*v*) CYP1A2 in untreated (CTL) and rifampicin-treated (RIF) samples from three conditions on day 7 following bioprinting. All gene expression fold changes are relative to the expressions of hiPSC-HPCs on day 12 of differentiation before bioprinting. Error bars represent SEM, and $n = 3$ for all data points.

not affect significantly the expression of CYP2B6 (Fig. 4 *D, iv*), which was previously reported to be induced by rifampicin in adult hepatocytes (41, 42). Taken together, these results showed that 3D triculture model provided an environment for hiPSC-HPCs that improved not only anabolic and catabolic functions, but also the key CYP expression levels and the drug induction potential.

Discussion

Recent approaches that used hiPSC-derived hepatic cells to develop personalized hepatic models have been largely limited to 2D or simple 3D culture and thus lost the liver structural and cellular composition information (3, 7, 10–14). The complex microarchitecture and cellular interactions in liver are thought to be essential to long-term hepatocyte functional maintenance as supported by many reports on the loss of liver-specific functions from hepatocytes taken out from the liver (5, 6). The purpose of this study was to develop a 3D in vitro hepatic model that patterns hiPSC-HPCs and the relevant supporting cells in a liver lobule-like structure and to investigate whether this 3D triculture model can promote hiPSC-HPCs maturation and functional preservation in the assigned 3D biomimetic structure.

The application of the rapid 3D bioprinting process to our study allows the flexible use of digital masks (21, 23, 24) and thus facilitates the process of liver lobule pattern design and modification. Moreover, the projection optics of the system focuses light patterns at micrometer-level resolution, thus enabling the biofabrication of the liver lobule hydrogel construct within several seconds with minimal UV illumination. The thickness of the construct, controlled by the motion controller of the system, can be flexibly adjusted based on various design criteria such as diffusion limitation in models where vascularized system is not fully developed or the large-scale construct in the case of fully vascularized models. As such, the rapid and highly flexible bioprinting system is an excellent tool for building 3D tissue constructs with physiologically relevant dimensions. The two complementary hexagonal patterns not only mimic the in vivo microarchitecture, but also enable both direct contacts at the pattern interface and possible local paracrine interactions between hepatic cells and supporting cells within the hexagons. The in vitro liver construct has its lobule diameter within the range of the healthy human liver lobule dimension. In addition to mimicking the native dimension, we also controlled the compressive moduli of the hydrogel matrices for both hepatic cells and supporting cells, because the matrix stiffness has been shown to strongly affect the functions of hepatocytes (27). We carefully adjusted the light exposure time and the percentage of photocross-linkable materials, the two critical factors in controlling the degree of cross-linking and thus the stiffness of the materials, so that the average compressive moduli of the hydrogel matrices mimicked that of the reported liver tissue (Fig. S1) (27).

In addition to the capability of building a system composed of the 3D hepatic construct, the use of hepatic cells from proper stages is also very important to the success of an in vitro liver model. The hepatic differentiation protocol used in our study is similar to that in many reports (7, 9). Our results of characterization of each differentiation stage by both immunofluorescent staining of key markers and expression levels of important genes are within the ranges of those observed in literature (7, 9), suggesting that the differentiation process has been successful. The characterizations of the cells along differentiation stages and before encapsulation by staining (Fig. 2*A*) and flow cytometry (Fig. S5) are important in controlling the quality and purity of hiPSC-HPCs for the bioprinting process and thus the functional performance of the model. Moreover, future study on the mesenchymal to epithelial transition process, which is omitted by many current hepatic differentiation protocols (7, 8, 12, 13), can be carried out to understand, in depth, the differentiation from HPCs to more mature hepatic epithelia. When assessing the albumin production levels of hiPSC-HPCs and HLCs following GelMA encapsulation, the higher magnitude and more sustained level of albumin produced following the peak by HPCs supported their potential to be better candidates for the 3D hydrogel encapsulation. This observation may be because HLCs in the later stage of the differentiation process are in a more mature status than HPCs (Fig. 2 *A* and *B*) and more metabolically active as in adult hepatocytes, and hence may not adapt to the encapsulated environment. Moreover, the fact that HPCs are maintained under hypoxia differentiation, whereas HLCs are cultured in nomoxia conditions, would facilitate the transition of the former into hydrogel encapsulation. The use of mature HLCs or adult hepatocytes in future models will require the incorporation of more specific endothelial cells such as LSECs to further facilitate the solute transport by their developed fenestration clusters and to provide cell interactions at the same developmental stage. In addition to characterizing key liver markers and metabolic product secretion, which we focused in this study, potential cholangiocytes derived from the bipotential hiPSC-HPCs may be further characterized in future studies. Such characterizations on biliary system, as well as further characterization of hepatic epithelia, are important in verifying a mature and functional liver model with biliary system.

Characterization of cell viability of hiPSC-HPCs showed that an acceptable number of cells remained viable following the whole process of bioprinting and also during the subsequent culture. In addition to knowing that most cells stayed viable, it is also important to understand the macroscopic changes of the construct over time. Interestingly, the construct, although appearing as a slab under brightfield, not only maintained the intrinsic hexagonal structures but also showed cell reorganization within them over time. The staining of E-cadherin and albumin expression over time demonstrated a cell–cell interaction and gradual maturation of HPCs. In line with aggregate formation, the realignment of supporting cells along the hydrogel lines can potentially facilitate channel formation and possible vascularization (31). The greater HPC aggregate size observed in this 3D triculture model further supports the beneficial effects from supporting cells as widely reported in 2D coculture models (14, 42).

In line with many structural changes observed, there are also functional advancements in HPCs cultured in the 3D triculture model. The increased expression of TTR in hiPSC-HPCs in 3D triculture correlated with that of HNF4a, which controls the expressions of both TTR and other hepatocyte nuclear factors that regulate the expression of several hepatic genes (30). The improved ALB expression also agrees with the increased albumin secretion from HPCs cultured in 3D triculture model 7 d following bioprinting. Despite the eventual decline in albumin and urea production, the relatively higher secretion level over time suggests that hiPSC-HPCs in 3D triculture model attained a more mature stage than those in merely 3D encapsulation or 2D monolayer culture. Finally, in addition to the higher expression levels of liver-specific genes, hiPSC-HPCs in 3D triculture model also have higher basal CYP expression, which is essential to drug metabolism. The higher basal CYP3A4 expression itself suggests a maturation toward adult hepatocytes as fetal hepatocytes express very low levels of CYP3A4 (43). The significant induction by rifampicin of CYP3A4, CYP2C9, and CYP2C19 expression levels shows that hiPSC-HPCs after 7 d in 3D triculture are able to respond positively to rifampicin as reported for primary hepatocytes (42), thus potentially improving the metabolism and clearance of the drug. Rifampicin is also an inducer of CYP2B6; therefore, the fact that rifampicin treatment did not lead to induction of CYP2B6 under any of the conditions suggests that hiPSC-HPCs at this stage may still be incompetent in terms of their drug metabolism capability. Further characterization on the RNA profiling of additional phase I and II enzymes and comparison with adult liver expression profiles can be carried out in future work to provide an in-depth understanding of the maturation level and the drug metabolizing capability of the model.

hiPSC-derived hepatic cells, despite their potential to have malignant transformation following in vivo transplantations, have been widely recognized as the most promising candidate for developing patient-specific human hepatic models in vitro (4, 7). Current in vitro liver models using hiPSC-derived hepatic cells are largely limited by their lack of biomimicry (3, 7, 10–14). The 3D triculture model presented here highlights the successful application of

DLP-based bioprinting technology to liver tissue engineering and thus the progress of the field to a level where the complex liver microarchitecture and cell composition can be studied in a physiologically relevant model. Further incorporation of functional and liver-specific vasculature based on LSECs and introduction of diseased cell types and extracellular environment during various development stages could open the door to establishing a more sophisticated, large-scale liver model with the potential to represent relevant diseases. The hepatic model developed in this study provides a 3D environment for hiPSC-derived hepatic cells in triculture with supporting cells in a hepatic lobule microarchitecture and has the ability to facilitate in vitro maturation and functional maintenance of hiPSC-derived hepatic cells in a biomimetic microenvironment. Hence, this model demonstrates great potential to serve as a patient-specific platform for pathophysiological studies, early drug screening, and clinical translation.

Materials and Methods

Detailed protocols for hiPSC generation, deriving hiPSC-hepatic cells, material synthesis and preparation, mechanical testing, 3D bioprinting, immunofluorescence imaging, gene expression analysis, and liver-specific metabolite secretion analysis are provided in *SI Materials and Methods*.

ACKNOWLEDGMENTS. We thank Peter Chung, Aditya Kumar, and Antony C. Chan for technical assistance and helpful discussions. This work was supported by National Institute of Biomedical Imaging and Bioengineering Grants R01EB012597 and R21EB017876. The University of California, San Diego Neuroscience Microscopy Shared Facility was supported by Grant P30 (NS047101) from the National Institutes of Health.

1. Kaplowitz N (2005) Idiosyncratic drug hepatotoxicity. *Nat Rev Drug Discov* 4(6): 489–499.
2. Guguen-Guillouzo C, Corlu A, Guillouzo A (2010) Stem cell-derived hepatocytes and their use in toxicology. *Toxicology* 270(1):3–9.
3. Yoon No D, Lee K-H, Lee J, Lee S-H (2015) 3D liver models on a microplatform: Well-defined culture, engineering of liver tissue and liver-on-a-chip. *Lab Chip* 15(19): 3822–3837.
4. Bhatia SN, Underhill GH, Zaret KS, Fox IJ (2014) Cell and tissue engineering for liver disease. *Sci Transl Med* 6(245):245sr2.
5. Sivaraman A, et al. (2005) A microscale in vitro physiological model of the liver: Predictive screens for drug metabolism and enzyme induction. *Curr Drug Metab* 6(6): 569–591.
6. Hewitt NJ, et al. (2007) Primary hepatocytes: Current understanding of the regulation of metabolic enzymes and transporter proteins, and pharmaceutical practice for the use of hepatocytes in metabolism, enzyme induction, transporter, clearance, and hepatotoxicity studies. *Drug Metab Rev* 39(1):159–234.
7. Schwartz RE, Fleming HE, Khetani SR, Bhatia SN (2014) Pluripotent stem cell-derived hepatocyte-like cells. *Biotechnol Adv* 32(2):504–513.
8. Mallanna SK, Duncan SA (2013) Differentiation of hepatocytes from pluripotent stem cells. *Curr Protoc Stem Cell Biol* 26:1G.4.1–1G.4.13.
9. Kondo Y, et al. (2014) An efficient method for differentiation of human induced pluripotent stem cells into hepatocyte-like cells retaining drug metabolizing activity. *Drug Metab Pharmacokinet* 29(3):237–243.
10. Takayama K, et al. (2013) 3D spheroid culture of hESC/hiPSC-derived hepatocyte-like cells for drug toxicity testing. *Biomaterials* 34(7):1781–1789.
11. Takebe T, et al. (2013) Vascularized and functional human liver from an iPSC-derived organ bud transplant. *Nature* 499(7459):481–484.
12. Du C, Narayanan K, Leong MF, Wan ACA (2014) Induced pluripotent stem cell-derived hepatocytes and endothelial cells in multi-component hydrogel fibers for liver tissue engineering. *Biomaterials* 35(23):6006–6014.
13. Takebe T, et al. (2014) Generation of a vascularized and functional human liver from an iPSC-derived organ bud transplant. *Nat Protoc* 9(2):396–409.
14. Berger DR, Ware BR, Davidson MD, Allsup SR, Khetani SR (2015) Enhancing the functional maturity of induced pluripotent stem cell-derived human hepatocytes by controlled presentation of cell-cell interactions *in vitro*. *Hepatology* 61(4):1370–1381.
15. Kim Y, Rajagopalan P (2010) 3D hepatic cultures simultaneously maintain primary hepatocyte and liver sinusoidal endothelial cell phenotypes. *PLoS One* 5(11):e15456.
16. Kim K, Ohashi K, Utoh R, Kano K, Okano T (2012) Preserved liver-specific functions of hepatocytes in 3D co-culture with endothelial cell sheets. *Biomaterials* 33(5): 1406–1413.
17. Khademhosseini A, Langer R, Borenstein J, Vacanti JP (2006) Microscale technologies for tissue engineering and biology. *Proc Natl Acad Sci USA* 103(8):2480–2487.
18. Faulkner-Jones A, et al. (2015) Bioprinting of human pluripotent stem cells and their directed differentiation into hepatocyte-like cells for the generation of mini-livers in 3D. *Biofabrication* 7(4):044102.
19. Liu Tsang V, et al. (2007) Fabrication of 3D hepatic tissues by additive photopatterning of cellular hydrogels. *FASEB J* 21(3):790–801.
20. Neiman JAS, et al. (2015) Photopatterning of hydrogel scaffolds coupled to filter materials using stereolithography for perfused 3D culture of hepatocytes. *Biotechnol Bioeng* 112(4):777–787.
21. Hribar KC, Soman P, Warner J, Chung P, Chen S (2014) Light-assisted direct-write of 3D functional biomaterials. *Lab Chip* 14(2):268–275.
22. Hribar KC, et al. (2015) Nonlinear 3D projection printing of concave hydrogel microstructures for long-term multicellular spheroid and embryoid body culture. *Lab Chip* 15(11):2412–2418.
23. Soman P, Chung PH, Zhang AP, Chen S (2013) Digital microfabrication of user-defined 3D microstructures in cell-laden hydrogels. *Biotechnol Bioeng* 110(11):3038–3047.
24. Gou M, et al. (2014) Bio-inspired detoxification using 3D-printed hydrogel nanocomposites. *Nat Commun* 5:3774.
25. Kim K, et al. (2014) 3D optical printing of piezoelectric nanoparticle-polymer composite materials. *ACS Nano* 8(10):9799–9806.
26. Rouvière O, et al. (2006) MR elastography of the liver: Preliminary results. *Radiology* 240(2):440–448.
27. You J, et al. (2013) Characterizing the effects of heparin gel stiffness on function of primary hepatocytes. *Tissue Eng Part A* 19(23-24):2655–2663.
28. Baier Leach J, Bivens KA, Patrick CW, Jr, Schmidt CE (2003) Photocrosslinked hyaluronic acid hydrogels: Natural, biodegradable tissue engineering scaffolds. *Biotechnol Bioeng* 82(5):578–589.
29. Si-Tayeb K, Lemaigre FP, Duncan SA (2010) Organogenesis and development of the liver. *Dev Cell* 18(2):175–189.
30. DeLaForest A, et al. (2011) HNF4A is essential for specification of hepatic progenitors from human pluripotent stem cells. *Development* 138(19):4143–4153.
31. Baranski JD, et al. (2013) Geometric control of vascular networks to enhance engineered tissue integration and function. *Proc Natl Acad Sci USA* 110(19):7586–7591.
32. Tsuji W, Rubin JP, Marra KG (2014) Adipose-derived stem cells: Implications in tissue regeneration. *World J Stem Cells* 6(3):312–321.
33. Tong JZ, Sarrazin S, Cassio D, Gauthier F, Alvarez F (1994) Application of spheroid culture to human hepatocytes and maintenance of their differentiation. *Biol Cell* 81(1):77–81.
34. Glicklis R, Merchuk JC, Cohen S (2004) Modeling mass transfer in hepatocyte spheroids via cell viability, spheroid size, and hepatocellular functions. *Biotechnol Bioeng* 86(6):672–680.
35. Chang TT, Hughes-Fulford M (2009) Monolayer and spheroid culture of human liver hepatocellular carcinoma cell line cells demonstrate distinct global gene expression patterns and functional phenotypes. *Tissue Eng Part A* 15(3):559–567.
36. Chang TT, Hughes-Fulford M (2014) Molecular mechanisms underlying the enhanced functions of three-dimensional hepatocyte aggregates. *Biomaterials* 35(7):2162–2171.
37. Luebke-Wheeler JL, Nedredal G, Yee L, Amiot BP, Nyberg SL (2009) E-cadherin protects primary hepatocyte spheroids from cell death by a caspase-independent mechanism. *Cell Transplant* 18(12):1281–1287.
38. Zhou SF, Liu JP, Chowbay B (2009) Polymorphism of human cytochrome P450 enzymes and its clinical impact. *Drug Metab Rev* 41(2):89–295.
39. Guengerich FP (1999) Cytochrome P-450 3A4: Regulation and role in drug metabolism. *Annu Rev Pharmacol Toxicol* 39:1–17.
40. Backman JT, Granfors MT, Neuvonen PJ (2006) Rifampicin is only a weak inducer of CYP1A2-mediated presystemic and systemic metabolism: Studies with tizanidine and caffeine. *Eur J Clin Pharmacol* 62(6):451–461.
41. Faucette SR, et al. (2004) Regulation of CYP2B6 in primary human hepatocytes by prototypical inducers. *Drug Metab Dispos* 32(3):348–358.
42. Khetani SR, Bhatia SN (2008) Microscale culture of human liver cells for drug development. *Nat Biotechnol* 26(1):120–126.
43. Hakkola J, et al. (2001) Cytochrome P450 3A expression in the human fetal liver: Evidence that CYP3A5 is expressed in only a limited number of fetal livers. *Biol Neonate* 80(3):193–201.
44. Fairbanks BD, Schwartz MP, Bowman CN, Anseth KS (2009) Photoinitiated polymerization of PEG-diacrylate with lithium phenyl-2,4,6-trimethylbenzoylphosphinate: Polymerization rate and cytocompatibility. *Biomaterials* 30(35):6702–6707.
45. Nichol JW, et al. (2010) Cell-laden microengineered gelatin methacrylate hydrogels. *Biomaterials* 31(21):5536–5544.
46. Corstorphine L, Sefton MV (2011) Effectiveness factor and diffusion limitations in collagen gel modules containing HepG2 cells. *J Tissue Eng Regen Med* 5(2):119–129.